On the Importance of Sea Surface Temperature for Aerosol-Induced Brightening of Marine Clouds and Implications for Cloud Feedback in a Future Warmer Climate

Xiaoli Zhou[1,2] , **Jianhao Zhang[1,2,3]** , and **Graham Feingold[1,2]**

[1]Chemical Sciences Laboratory, NOAA, Boulder, CO, USA, [2]Cooperative Institute for Research in Environmental Sciences (CIRES), University of Colorado, Boulder, CO, USA, [3]National Research Council, National Academies of Sciences, Engineering, Medicine (NASEM), Washington, DC, USA

Abstract Marine low clouds are one of the greatest sources of uncertainty for climate projection. We present an observed climatology of cloud albedo susceptibility to cloud droplet number concentration perturbations (S_0) with changing sea surface temperature (SST) and estimated inversion strength for single-layer warm clouds over the North Atlantic Ocean, using eight years of satellite and reanalysis data. The key findings are that SST has a dominant control on S_0 in the presence of co-varying synoptic conditions and aerosol perturbations. Regions conducive to aerosol-induced darkening (brightening) clouds occur with high (low) local SST. Higher SST significantly hastens cloud-top evaporation with increasing aerosol loading, by accelerating entrainment and facilitating entrainment drying. In a global-warming-like scenario where aerosol loading is reduced, less cloud darkening is expected, mainly as a result of reduced entrainment drying. Our results imply a less positive low-cloud liquid water path feedback in a warmer climate with decreasing aerosol loading.

Plain Language Summary Low clouds over the ocean are a poorly quantified component of the climate system. Here we use eight years of space-based measurements and meteorological data to quantify how the brightness of single-layer low clouds over the North Atlantic Ocean might respond to cloud droplet number concentration perturbations in a warmer world. We find that under higher sea surface temperatures, increases in drop number tend to reduce cloud brightness by accelerating evaporation of cloud water. Thus in a warmer world, low clouds will reflect less energy to space in response to an increase in aerosol loading. If aerosol sources decrease then we expect more robust clouds and more offsetting of greenhouse gas warming.

1. Introduction

Marine low clouds are ubiquitous over the subtropical and midlatitude oceans (Wood, 2012) and strongly regulate the Earth's radiation budget by reflecting solar radiation back to space (Klein & Hartmann, 1993; Stephens et al., 2012). How low clouds will respond to changes in regional and global climate change is still uncertain and constitutes a major uncertainty in predictions of climate sensitivity (Bony & Dufresne, 2005; Dufresne & Bony, 2008; Vial et al., 2013; Zelinka et al., 2020). A primary source of spread in general circulation model (GCM)-derived climate sensitivity is the entrainment process at cloud top (Bretherton & Blossey, 2014; Bretherton et al., 2013; Caldwell et al., 2013; Rieck et al., 2012; Sherwood et al., 2014; M. Zhang et al., 2013), which responds to changes in sea surface temperature (SST) and lower tropospheric stability (LTS, Ceppi & Nowack, 2021; Qu et al., 2015) under global warming. Recent observational constraint studies predict positive shortwave cloud feedbacks across the subtropics and midlatitudes (Ceppi & Nowack, 2021; Myers & Norris, 2016; Myers et al., 2021) due to a decrease in boundary layer cloud cover (McCoy et al., 2017; Qu et al., 2015; Zhai et al., 2015). This decrease in cloudiness is corroborated by long-term trends in observed cloud cover (Norris et al., 2016).

The uncertainty in climate projection is exacerbated by the effect of anthropogenic atmospheric aerosols on global cloud radiative forcing through changes in cloud amount and brightness. One of the strongest aerosol indirect effects occurs via changes in cloud condensate (Albrecht, 1989), which is typically quantified via observations of the response of cloud liquid water path (CWP) to aerosol-induced perturbations (Chen et al., 2014). Chen et al. (2014) identify LTS and free tropospheric relative humidity (RH_{ft}) as important controls on the aerosol-induced cloud water adjustment and the strength of aerosol-cloud radiative forcing. They find that for a drier free troposphere and LTS, CWP decreases with increasing aerosol due to a strengthened entrainment rate and evaporation efficiency induced by smaller cloud droplets (i.e., greater droplet surface areas) and weaker sedimentation

(evaporation-entrainment feedbacks, Ackerman et al., 2004; Wang et al., 2003), which could counter the Twomey effect (enhanced albedo from more but smaller droplets; Twomey, 1974) and lead to lower cloud albedo (A_c). Existing studies only partially address the difficult problem of causality. How the governing meteorological factors co-vary with each other and with aerosol perturbations, and how cloud water adjustment is related to greenhouse gas-warming-induced changes is barely discussed in the literature. The latter is neglected in the current method of diagnosing aerosol forcing in GCMs (Mülmenstädt & Feingold, 2018).

In this study, we present an observed climatology of A_c susceptibility to cloud droplet number concentration (N_d) perturbations with changing SST and estimated inversion strength (EIS; Wood & Bretherton, 2006)–two key meteorological cloud-controlling factors (Ceppi & Nowack, 2021; Klein et al., 2017; Qu et al., 2015), for single-layer warm (liquid-phase) clouds in the planetary boundary layer (PBL) over the North Atlantic Ocean, where there exists a wide range of SST. We show that, regardless of EIS, SST has a strong influence on the relative occurrence of aerosol-induced cloud brightening on daily and inter-annual timescales by modulating inversion stability and cloud-top humidity. Our results suggest that in a future warmer climate where aerosol loading is expected to reduce, there will be a more frequent occurrence of more reflective clouds (brightening). The results presented here might be linked to a less positive low-cloud liquid water path feedback in a warmer climate with decreasing aerosol loading.

2. Data Set Description

We use 8 years (2003–2011) of the National Aeronautics and Space Administration (NASA) A-Train satellite measurements and European Center for Medium range Weather Forecast (ECMWF)'s fifth generation atmospheric reanalysis (ERA5) over the North Atlantic Ocean (25°N 55°N; 50°W 15°W) for single-layer liquid phase clouds.

Cloud properties including cloud water path (CWP), cloud optical depth, effective radius of cloud droplets, cloud top height and temperature, cloud phase, and cloud layers are sourced from Collection 6.1 daytime (~13:30 p.m. local time) marine cloud retrievals at 1 km (nadir) resolution from MODerate-resolution Imaging Spectroradiometer (MODIS) on the Aqua satellite. All cloud properties are averaged over the footprint (~20 km) of the Clouds and Earth's Radiant Energy System (CERES; Minnis et al., 2020). The CERES footprint-level cloud property products are included in the CERES Single Scanner Footprint (SSF) level 2 Edition 4A data set.

Rain rate data is sourced from the Advanced Microwave Scanning Radiometer for Earth Observing System (AMSR-E; Wentz & Meissner, 2004), provided on a non-uniform grid within a 1,445 km-wide swath with a pixel resolution of ~10 km at the center of the track.

We derive N_d using visible cloud optical depth and effective radius of cloud droplets measured in the 3.7 m channel following Grosvenor et al. (2018). To reduce errors in N_d retrievals, we confine our analysis to full coverage (100% cloud cover within the CERES footprint where the cloud scenes tend to be more homogeneous), single-layer liquid phase clouds with cloud top height no greater than 2 km and cloud top temperature no less than 273 K. Clouds with optical depth less than 1 are considered too thin for a reliable N_d retrieval and are therefore removed from the analysis. Only N_d retrievals less than 600 cm^{-3} are used in this study.

Since this study focuses on full cloud coverage within the CERES footprint, we estimate A_c from the all-sky albedo computed as the ratio of upward to incoming solar irradiance at the top-of-atmosphere (TOA) measured by CERES. The computed A_c is normalized by its value at 0 solar zenith angle (SZA). We restrict the SZA to less than 65 for reliable albedo calculation.

The environmental conditions are sourced from ERA5 reanalysis with a resolution of 0.25. The inversion strength is estimated from EIS derived from the ERA5 temperature at the surface and at 700 hPa following Wood and Bretherton (2006). As a refinement of LTS, EIS is a better predictor of inversion strength over the midlatitude oceans, where the free troposphere is cooler than in the tropics. Since we focus on boundary layer clouds below 2 km, we consider the absolute (relative) humidity at 800 hPa from ERA5 as a proxy for the free tropospheric absolute (relative) humidity. We compute the 900 hPa aerosol number concentration (N_a) from ERA5 aerosol mass at 900 hPa following Boucher and Lohmann (1995). Using vertical temperature and humidity profiles from ERA5, we identify the inversion as the level around the maximum increase in temperature with a height
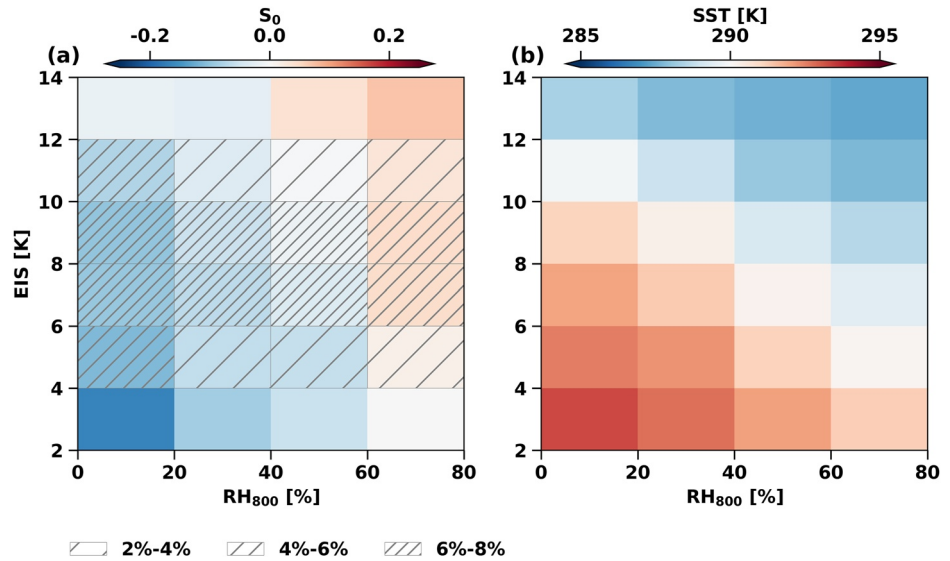
Figure 1. (a) The mean values of susceptibility of cloud albedo to the cloud droplet number concentration (S_0) within bins of estimated inversion strength (EIS) and relative humidity at 800 hPa (RH_{800}). The bin width is 2K ΔEIS in the vertical and 20% Δ RH_{800} in the horizontal. At least 20 samples are required in each bin. Hatches in (a) indicate the frequency of occurrence in each bin. Bins with no hatching have a frequency of occurrence below 2%. The averaged standard deviation of S_0 in each bin is 0.2. (b) Same as (a) but for sea surface temperature (SST). The averaged standard deviation of SST in each bin is 2.5 K.

that occurs below 2 km, and has an increase in temperature and a decrease in absolute humidity (Rémillard et al., 2012; Zhou et al., 2015). The SST is sourced from ERA5.

To merge the CERES footprint level data, AMSR-E rain rate data, and ERA5 reanalysis in the same study, we re-grid all data onto the CERES resolution (0.2°) using nearest-neighbor interpolation. We further divide the data into 2° × 2° latitude-longitude scenes. In each scene where scene-level cloud fraction (f_c) is greater than 0.25, the natural log of A_c from cloudy pixels is regressed onto the natural log of N_d. The resulting linear regression coefficient is an estimate of $S_0 = d\ln(A_c)/d\ln(N_d)$, defined as the A_c susceptibility to N_d perturbations. The logarithmic form reduces the sensitivity of S_0 to the measurement accuracy of A_c and N_d. The 2° × 2° scene is big enough to include variability in cloud properties, and small enough to guarantee nearly homogeneous meteorological conditions within the scene, such that the regression coefficients computed from the satellite swaths can be reasonably considered as the sensitivity of A_c to an N_d perturbation for a certain meteorological state. All other variables including SST, EIS, CWP, cloud top height (a proxy for inversion height), rain rate, absolute humidity at 800 hPa (q_{800}) and at the inversion (q_{inv}), relative humidity at 800 hPa (RH_{800}) and at 1,000 hPa (RH_{1000}), N_d, and N_a at 900 hPa are averaged in cloudy pixels for each scene. In total, 6,562 samples are included. It is possible that the large-scale forcing might not be equilibrated with cloud properties, which is also common in the mean state of the climate. The corresponding cloud radiative susceptibility at TOA is estimated from cloudy pixels in each scene following $F_c = -dA_c/d\ln(N_d)SW\downarrow_{TOA}$ [W m^{-2}ln(N_d)$^{-1}$], where SW$\downarrow_{TOA}$ is downward shortwave radiation at TOA.

3. Results

Bin-averaged S_0 with respect to EIS and RH_{800} in our study (Figure 1a) resembles closely Figure 1 in Chen et al. (2014), supporting the finding that darkening clouds (defined as negative S_0) are favored by dry overlying air and a relatively unstable boundary layer. Over 64% of the samples are of EIS between 4 and 12 K, with RH_{800} varying widely from 0% to 80% (Figure 1a). The frequency-weighted average S_0 over the North Atlantic is −0.03, corresponding to an F_c of 12 W m^{-2}ln(N_d)$^{-1}$. Comparing Figure 1b with Figure 1a shows that bin-averaged SST over the North Atlantic varies with an almost opposite trend to S_0 with respect to EIS and RH_{800}, suggesting that SST has a strong control on the aerosol-induced brightness of marine clouds over the North Atlantic Ocean by modulating LTS and free tropospheric relative humidity (RH). Regions prone to an aerosol-related darkening of clouds occur at high local SST.
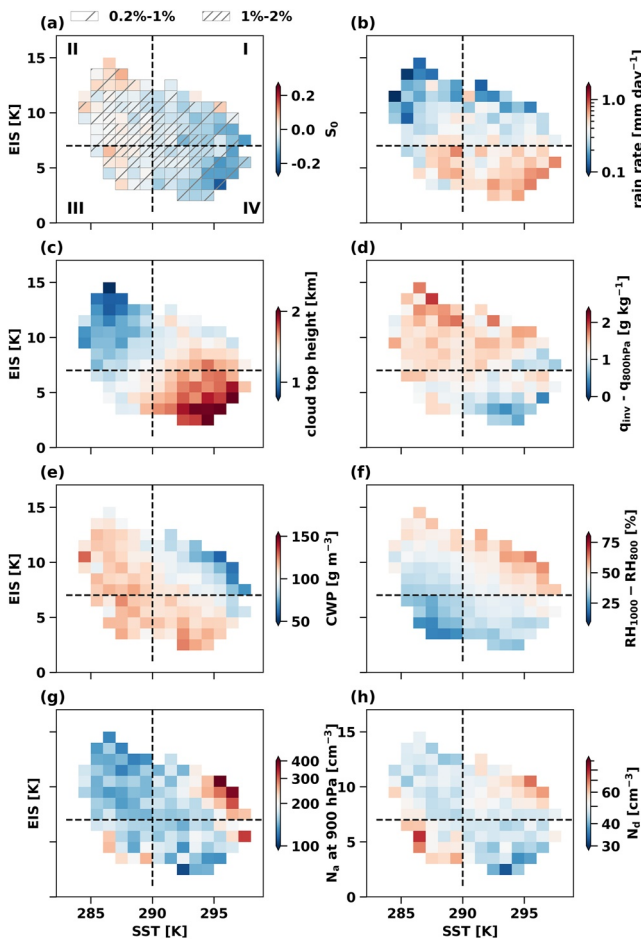
Figure 2. The mean values of (a) susceptibility of cloud albedo to cloud droplet number concentration(S_0), (b) rain rate, (c) cloud top height, (d) absolute humidity difference between inversion top (q_{inv}) and 800 hPa (q_{800}), (e) cloud water path (CWP), (f) relative humidity difference between 1,000 hPa (RH_{1000}) and 800 hPa (RH_{800}), (g) aerosol number concentration at 900 hPa (N_a), and (h) cloud droplet number concentration (N_d) within bins of estimated inversion strength and sea surface temperature. The bin width is 1K ΔEIS in the vertical and 1K ΔSST in the horizontal. At least 20 samples are required in each bin. Black dashes indicate SST = 290 K and EIS = 7 K isolines. The Roman numerals I, II, III, and IV in (a) indicate quadrants. Hatches in (a) indicate the frequency of occurrence in each bin. The bins with no hatching have a frequency of occurrence below 0.2%.

The control of SST on S_0 is seen clearly in Figure 2a where S_0 is now plotted in the EIS - SST space. The bin-averaged S_0 is predominantly negative (darkening) for SST > 290 K, regardless of EIS. For SST < 290 K, S_0 is mostly positive or near zero. EIS appears to be a good indicator of warm precipitation (Figure 2b), such that relatively high EIS (EIS > 7 K) is associated with none or very lightly precipitating clouds (rain rate < 0.3 mm day^{-1}) and precipitation tends to increase with decreasing EIS. In this sense, the EIS - SST space can be broadly divided into four Quadrants—Quadrant I (upper right): nonprecipitating darkening clouds, Quadrant II (upper left): nonprecipitating brightening clouds, Quadrant III (lower left): precipitating brightening clouds, and Quadrant IV (lower right): precipitating darkening clouds. It can be inferred from Figures 2a and 2b that the aerosol-induced brightening of marine clouds is not directly related to the occurrence of precipitation. We will elaborate below on why darkening clouds tend to occur in Quadrants I & IV where SST is relatively high.

A notable change in S_0 can be seen along the diagonal from the top left to the bottom right corner in the EIS-SST space where EIS is negatively correlated with SST (free tropospheric temperature maintains relatively unchanged). This is a typical pathway of eastern subtropical stratocumulus when advected equatorward by the easterly trade winds. All else equal, higher local SST deepens the boundary layer by reducing EIS along the diagonal (Figure 2c). The deepening boundary layer is associated with reduced cloud top absolute humidity (Figure 2d) since in nature free tropospheric absolute humidity tends to decrease with height. Our results show that a ~1 km deeper boundary layer corresponds to a ~2 g kg^{-1} reduction in the cloud top absolute humidity. The relatively unstable lower troposphere and drier overlying air serve to accelerate cloud-top entrainment and facilitate cloud top evaporation and therefore favor cloud darkening.

Even with the strong difference in cloud top heights, the bin-averaged CWPs along the diagonal are comparable (Figure 2e), likely due to the counteracting effects of a deeper inversion layer and higher cloud base at lower EIS. This suggests that the radiative cooling driving cloud-top turbulence is not the dominant control on the entrainment along the diagonal. We also examine the influence of precipitation scavenging of cloud water on cloud darkening in Quadrant IV and find that precipitation is not significant enough to play a role (Text S1, Figures S1 and S2 in Supporting Information S1). The above result suggests that the response of cloud albedo to the perturbed N_d is expected to be stronger along the prevailing winds when the underlying sea surface becomes warmer, at least for non-precipitating or lightly precipitating stratocumulus clouds.

If the free tropospheric temperature changes at a similar or faster rate than the SST, as in a global warming scenario or seasonal change (e.g., Qu et al., 2014, 2015; Wood & Bretherton, 2006), EIS would change only marginally or positively with SST. This corresponds to a horizontal or diagonal from bottom left to top right corner in the EIS-SST space in Figure 2, along which S_0 also changes noticeably.

In this aforementioned scenario, assuming the same absolute humidity, higher SST corresponds to warmer free tropospheric air, which can dramatically decrease free tropospheric RH as per the Clausius-Clapeyron scaling (Figure S3 in Supporting Information S1), and thereby enhance entrainment drying of the boundary layer. The drier boundary layer triggers an increase in latent heat fluxes (LHF), which weakens the RH reduction in the boundary layer (Figure S3 in Supporting Information S1). This leads to an increased humidity difference between dry free tropospheric air and boundary layer air with increasing SST (Figure 2f). The stronger humidity difference at the inversion (ΔRH) is known to decrease low cloud fraction and amount through cloud top entrainment

(Bretherton et al., 2013; Lock, 2009; Qu et al., 2015). Here we show that the ΔRH also facilities negative S_0 and might further strengthen the positive cloud liquid water path feedback with increasing aerosol levels. Regions of high SST and EIS (Quadrant I) are associated with the warmest and thus driest free tropospheric air and hence experience the strongest ΔRH at cloud top (Figure 2f).

With the increase in ΔRH (and also LHF) in this scenario, CWP reduces correspondingly (Figure 2e). This is attributable to an increase in the LHF-induced in-cloud buoyancy fluxes, such that a small CWP is enough to generate comparable cloud top turbulence to sustain the boundary layer (Bretherton et al., 2013). These comparable levels of turbulence translate to similar entrainment rates; therefore it is the enhanced entrainment drying, rather than entrainment rate, that facilitates the cloud darkening. Note that when CWP is very low ($<50 \sim 60$ g m^{-2}), negative cloud adjustment is more than overcome by the enhanced Twomey effect and therefore S_0 becomes positive (J. Zhang et al., 2021).

The two scenarios discussed above suggest that under a future warmer climate, we expect more darkening (brightening) clouds with increasing (decreasing) aerosol loading. The responses are more significant for the stratocumulus clouds along the easterly trade winds.

The background aerosol concentrations are in general quite homogeneous over the North Atlantic region, except in Quadrants I and III where the bin-averaged N_a are slightly higher (Figure 2g). This is due to a slightly higher frequency of occurrence of large N_a ($N_a > 200$ cm^{-3}) in Quadrants I and III ($\sim 30\%$) compared to the other Quadrants ($\sim 20\%$). The higher N_a emanates from the European Continent and Greenland via favorable synoptic patterns (Figure S4 in Supporting Information S1). As a result, the bin-averaged N_d is slightly higher in Quadrants I and III (Figure 2h).

N_d is one of the important cloud properties (the other is CWP) that can directly modify S_0, by determining cloud droplet sedimentation velocity, precipitation, and the Twomey effect. We do find a negative correlation between S_0 and N_d over the North Atlantic. Clouds with low N_d (<30 cm^{-3}) tend to be associated with positive S_0 (Figure S5 in Supporting Information S1), which we attribute to be mainly driven by reduced evaporation-entrainment feedbacks and enhanced precipitation suppression when rain is present. Further analysis shows that the decreasing trend of S_0 with SST is not sensitive to the natural N_d variation (Figures S6–S8 in Supporting Information S1). This reflects the governing of S_0 by large-scale environmental conditions in the presence of local aerosol perturbations. The frequency-weighted averaged S_0 (F_c), however, is sensitive to N_d: S_0 (F_c) is 0.05 (-12 W m^{-2} ln(N_d)$^{-1}$), -0.08 (24 W m^{-2} ln(N_d)$^{-1}$), and -0.04 (19 W m^{-2} ln(N_d)$^{-1}$) for $N_d < 30$ cm^{-3}, $30 \leq N_d < 60$ cm^{-3}, $N_d \geq 60$ cm^{-3} respectively.

4. Seasonal and Inter-Annual Variability

The control of SST on S_0 is affected by the free tropospheric absolute humidity, which is tightly correlated with the seasonal variability in the Hadley circulation. In winter, the zonally averaged Hadley circulation is stronger and solar insolation is weaker (i.e., colder air), leading to drier free tropospheric air in the Northern Hemisphere subtropics as per the Clausius-Clapeyron relation. As a result, the q_{800} in June, July, and August (JJA) is ~ 5 g kg^{-1}, about three times as much as that in December, January, and February (DJF) (~ 1.5 g kg^{-1}) (Figure 3a).

Warmer free tropospheric air in JJA due to stronger solar radiation reduces the difference in free tropospheric RH between the seasons, although JJA is still significantly moister (Figure 3b). Warmer free tropospheric air in JJA also leads to a stronger EIS across all SST compared to DJF (Figure 3c), both of which inhibit cloud top entrainment and evaporation, lowering the boundary layer height (Figure 3d) and hampering cloud darkening in JJA.

N_d over the North Atlantic also appears to be seasonally dependent; N_d increases by nearly 25% in JJA, and amplifies with SST (Figure 3e). The increase in N_d with SST in JJA relative to DJF counteracts their difference in environmental conditions by enhancing evaporation-entrainment feedbacks. The counteracting effects of microphysical (N_d) and environmental (q_{800}, EIS) controls result in a comparable trend of S_0 with respect to SST in winter and in summer. There is a slightly more frequent occurrence of darkening clouds in winter as indicated by the close spacing between dots and shift of the blue shading toward negative S_0, suggesting a slightly more dominant influence of environmental control over microphysical control on S_0.
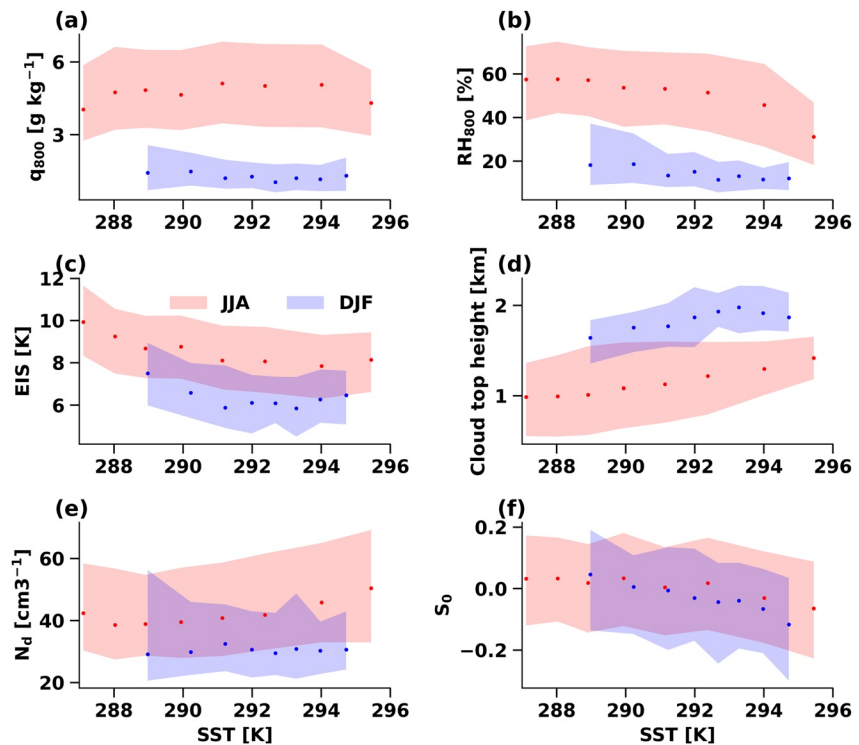
Figure 3. Quartiles of (a) absolute humidity at 800 hPa (q_{800}), (b) relative humidity at 800 hPa (RH$_{800}$), (c) estimated inversion strength (EIS), (d) cloud top height, (e) cloud droplet number concentration (N_d), and (f) susceptibility of cloud albedo to cloud droplet number concentration (S_0), within sea surface temperature (SST) bins for June, July, and August (JJA, red) and December, January, and February (DJF, blue). Dots indicate median values within SST bins (10%).

The control of SST on S_0 is shown to be much more significant than the control of N_d at the inter-annual time scale. S_0 shows an apparent anti-correlation with SST in both seasons (with a correlation coefficient R ∼ −0.4), especially in DJF when the year-to-year SST spans a greater range (Figure 4). Note that SST in Figure 4 is an average over the cloudy scenes and should not be interpreted as the annual mean SST in the North Atlantic area.

5. Discussion

The wide spatial variability in SST over the North Atlantic Ocean has allowed us to examine the response of S_0 to varying SST environments that are less contaminated by the seasonal co-variability between meteorological conditions. In regions with more homogeneous SST (e.g., the North Eastern Pacific Ocean (NEP); J. Zhang et al., 2021), the seasonal co-variation of SST with free tropospheric absolute humidity is remarkable, in a way that high (low) SST correlates with more (less) humid overlying air in summer (winter) when solar radiation is stronger (weaker) and the Hadley circulation is weaker (stronger). The humid free tropospheric air at high SST prevents efficient cloud top evaporation and offsets to a large extent the response of S_0 to changing SST. This is likely the reason why the controlling role of SST is not reflected in the NEP (J. Zhang et al., 2021) and other stratocumulus–dominant regions (Qu et al., 2015). Nevertheless, we expect clouds in these regions to respond similarly to those over the North Atlantic Ocean under global warming.

We note that this study only looks at full coverage clouds at the CIRES pixel level (∼20 km), which eliminates most of the low coverage open cell regime where it is more common to find enhanced precipitation. As a result, the clouds in this study are mostly precipitation free or lightly precipitating (92% of samples have rain rate <1 mm day^{-1}), such that aerosol-related increases in cloud water accompanying suppressed precipitation are less than cloud water losses associated with increased cloud-top entrainment. Clouds with more enhanced precipitation (lower N_d) are found to brighten with an increase in aerosol loading (Christensen & Stephens, 2012; J. Zhang et al., 2021).
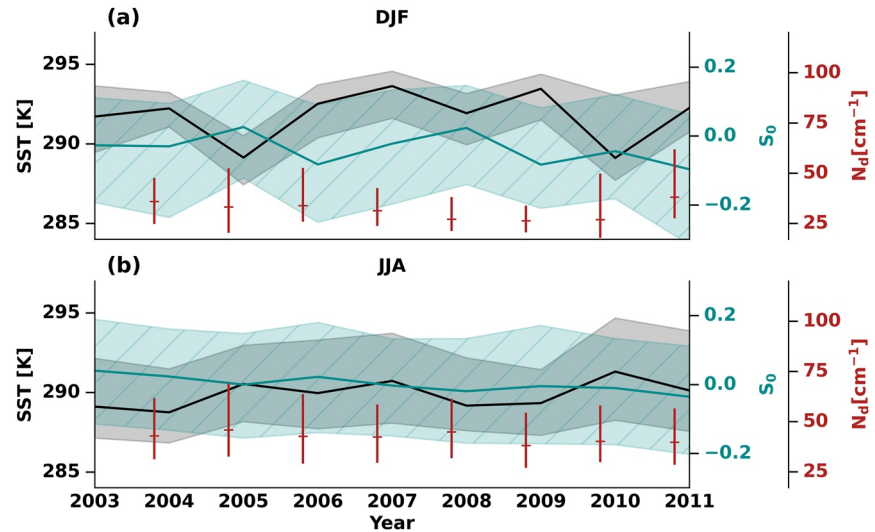
Figure 4. The annual median (solid line) and interquartile ranges (shading) of sea surface temperature (SST, black) and susceptibility of cloud albedo to cloud droplet number concentration (S_0, dark blue) for (a) December, January, and February (DJF) and (b) June, July, and August (JJA) from 2003 to 2011. The annual medians and interquartile ranges of cloud droplet number concentration (N_d) are indicated by red horizontal and vertical line markers.

The domain-averaged S_0 (−0.03) and F_c (12 W m^{-2} ln(N_d)$^{-1}$) are calculated from cloudy pixels in each scene. Considering the mean cloud fraction in each scene ($\sim$0.5), the radiative susceptibility due to the combined cloud water adjustment and Twomey effect over the North Atlantic is 6.9 W m^{-2}ln(N_d)$^{-1}$. This number might be less negative if scenes with cloud fraction less than 0.25 are included. The adjustment of cloud fraction to N_d might also affect the total radiative aerosol effect, but we are not able to address this information using the current data set.

The analysis shown in this study includes samples with all possible correlation coefficients between cloud albedo and N_d. A stricter refinement (e.g., |R| > 0.5) leads to more negative S_0 (−0.06) and F_c (22.7 W m^{-2}ln(N_d)$^{-1}$), and a stronger dependence of S_0 on SST (Figure S9 in Supporting Information S1). With the current data set, we cannot assess the diurnal variability of S_0, nor can we assess how S_0 responds to increased CO_2, whose direct radiative effect (downwelling longwave radiation) is thought to reduce the cloud-top radiative cooling and therefore thin the clouds (Bretherton et al., 2013). Further observational or numerical studies are encouraged in this regard.

6. Conclusions

This study presents an observed climatology of the marine cloud albedo susceptibility to perturbations in cloud droplet number concentration (S_0) and its relation to SST and related environmental conditions, using eight years of A-Train satellite measurements and reanalysis data. We find a strong control of SST on S_0; higher SST facilitates a greater entrainment rate (by increasing boundary layer instability) and entrainment drying (by deepening the cloud layer and creating a stronger humidity gradient at the inversion), both of which hasten evaporation at cloud top. With increasing aerosol burden, the evaporation is further enhanced via evaporation-entrainment feedbacks. As a result, higher SST is associated with a higher frequency of less reflective clouds and thus more negative S_0 with increasing aerosol loading. The exception is when clouds are very thin with CWP < 50 $\sim$ 60 g m^{-2}. We expect the response of clouds to a warming SST and aerosol perturbations to be broadly robust along the prevailing winds and under global warming, when clouds are not strongly precipitating.

We find that the aerosol perturbation is more locally confined and therefore more than offset by the perturbations of SST-induced environmental conditions and their control on S_0. Seasonal and inter-annual variability in SST and S_0 support our findings. Synoptic disturbances could affect the frequency of occurrence of clouds with different degrees of precipitation and brightness, but they are less important in determining cloud albedo susceptibility compared to the large-scale environmental conditions (e.g., seasonal variability; local SST) (Figure S4 in Supporting Information S1).

Projecting these results to a global-warming-like scenario where free tropospheric temperature changes at a similar or faster rate than SST, surface humidity is likely to increase at a higher rate than free tropospheric humidity according to the Clausius-Clapeyron relation (Bretherton et al., 2013; Qu et al., 2015), and the relative humidity of mixed air parcels at the inversion is likely to reduce (Rieck et al., 2012). As a result, the moisture contrast would still be enhanced, leaving clouds more vulnerable to evaporation. Our results provide insights into a future where if (a) (the more likely situation) anthropogenic aerosol emissions are reduced, the aerosol forcing associated with aerosol-cloud interactions will decrease in the eastern subtropical and midlatitude regions, and even more so along the easterly trade winds, thereby mitigating the positive cloud liquid water path feedback; or conversely if (b) a warmer climate the aerosol forcing associated with aerosol-cloud interactions will increase, leading to a more positive cloud liquid water path feedback.

Data Availability Statement

We acknowledge the Clouds and Earth's Radiant Energy System (CERES)'s Single Scanner Footprint (SSF) level 2 Edition 4A data set at https://ceres-tool.larc.nasa.gov/ord-tool/products?CERESProducts=SSFlevel2_Ed4); the European Center for Medium range Weather Forecast (ECMWF)'s fifth generation atmospheric reanalysis (ERA5) data at https://cds.climate.copernicus.eu/cdsapp#!/dataset/reanalysis-era5-pressure-levels?tab=overview; the Advanced Microwave Scanning Radiometer for Earth Observing System rain rate data at https://nsidc.org/data/AE_Rain.

References

Ackerman, A. S., Kirkpatrick, M. P., Stevens, D. E., & Toon, O. B. (2004). The impact of humidity above stratiform clouds on indirect aerosol climate forcing. *Nature*, *432*(7020), 1014–1017. https://doi.org/10.1038/nature03174

Albrecht, B. A. (1989). Aerosols, cloud microphysics, and fractional cloudiness. *Science*, *245*(4923), 1227–1230. https://doi.org/10.1126/science.245.4923.1227

Bony, S., & Dufresne, J.-L. (2005). Marine boundary layer clouds at the heart of tropical cloud feedback uncertainties in climate models. *Geophysical Research Letters*, *32*(20), L20806. https://doi.org/10.1029/2005gl023851

Boucher, O., & Lohmann, U. (1995). The sulfate-ccn-cloud albedo effect. *Tellus B: Chemical and Physical Meteorology*, *47*(3), 281–300. https://doi.org/10.3402/tellusb.v47i3.16048

Bretherton, C. S., & Blossey, P. N. (2014). Low cloud reduction in a greenhouse-warmed climate: Results from lagrangian les of a subtropical marine cloudiness transition. *Journal of Advances in Modeling Earth Systems*, *6*(1), 91–114. https://doi.org/10.1002/2013ms000250

Bretherton, C. S., Blossey, P. N., & Jones, C. R. (2013). Mechanisms of marine low cloud sensitivity to idealized climate perturbations: A single-les exploration extending the cgils cases. *Journal of Advances in Modeling Earth Systems*, *5*(2), 316–337. https://doi.org/10.1002/jame.20019

Caldwell, P. M., Zhang, Y., & Klein, S. A. (2013). Cmip3 subtropical stratocumulus cloud feedback interpreted through a mixed-layer model. *Journal of Climate*, *26*(5), 1607–1625. https://doi.org/10.1175/jcli-d-12-00188.1

Ceppi, P., & Nowack, P. (2021). Observational evidence that cloud feedback amplifies global warming. *Proceedings of the National Academy of Sciences*, *118*(30). https://doi.org/10.1073/pnas.2026290118

Chen, Y.-C., Christensen, M. W., Stephens, G. L., & Seinfeld, J. H. (2014). Satellite-based estimate of global aerosol–cloud radiative forcing by marine warm clouds. *Nature Geoscience*, *7*(9), 643–646. https://doi.org/10.1038/ngeo2214

Christensen, M. W., & Stephens, G. L. (2012). Microphysical and macrophysical responses of marine stratocumulus polluted by underlying ships: 2. Impacts of haze on precipitating clouds. *Journal of Geophysical Research: Atmosphere*, *117*(D11), D11203. https://doi.org/10.1029/2011jd017125

Dufresne, J.-L., & Bony, S. (2008). An assessment of the primary sources of spread of global warming estimates from coupled atmosphere–ocean models. *Journal of Climate*, *21*(19), 5135–5144. https://doi.org/10.1175/2008jcli2239.1

Grosvenor, D. P., Sourdeval, O., Zuidema, P., Ackerman, A., Alexandrov, M. D., Bennartz, R., et al. (2018). Remote sensing of droplet number concentration in warm clouds: A review of the current state of knowledge and perspectives. *Reviews of Geophysics*, *56*(2), 409–453. https://doi.org/10.1029/2017rg000593

Klein, S. A., Hall, A., Norris, J. R., & Pincus, R. (2017). Low-cloud feedbacks from cloud-controlling factors: A review. *Shallow clouds, water vapor, circulation, and climate sensitivity* (pp. 135–157). https://doi.org/10.1007/978-3-319-77273-8_7

Klein, S. A., & Hartmann, D. L. (1993). The seasonal cycle of low stratiform clouds. *Journal of Climate*, *6*(8), 1587–1606. https://doi.org/10.1175/1520-0442(1993)006<1587:tscols>2.0.co;2

Lock, A. (2009). Factors influencing cloud area at the capping inversion for shallow cumulus clouds. *Quarterly Journal of the Royal Meteorological Society: A journal of the atmospheric sciences, applied meteorology and physical oceanography*, *135*(641), 941–952. https://doi.org/10.1002/qj.424

McCoy, D. T., Eastman, R., Hartmann, D. L., & Wood, R. (2017). The change in low cloud cover in a warmed climate inferred from airs, modis, and era-interim. *Journal of Climate*, *30*(10), 3609–3620. https://doi.org/10.1175/jcli-d-15-0734.1

Minnis, P., Sun-Mack, S., Chen, Y., Chang, F.-L., Yost, C. R., Smith, W. L., et al. (2020). Ceres modis cloud product retrievals for edition 4—Part i: Algorithm changes. *IEEE Transactions on Geoscience and Remote Sensing*, *59*(4), 2744–2780.

Mülmenstädt, J., & Feingold, G. (2018). The radiative forcing of aerosol–cloud interactions in liquid clouds: Wrestling and embracing uncertainty. *Current Climate Change Reports*, *4*(1), 23–40. https://doi.org/10.1007/s40641-018-0089-y

Myers, T. A., & Norris, J. R. (2016). Reducing the uncertainty in subtropical cloud feedback. *Geophysical Research Letters*, *43*(5), 2144–2148. https://doi.org/10.1002/2015gl067416

Myers, T. A., Scott, R. C., Zelinka, M. D., Klein, S. A., Norris, J. R., & Caldwell, P. M. (2021). Observational constraints on low cloud feedback reduce uncertainty of climate sensitivity. *Nature Climate Change*, *11*(6), 501–507. https://doi.org/10.1038/s41558-021-01039-0

Norris, J. R., Allen, R. J., Evan, A. T., Zelinka, M. D., O'Dell, C. W., & Klein, S. A. (2016). Evidence for climate change in the satellite cloud record. *Nature*, *536*(7614), 72–75. https://doi.org/10.1038/nature18273

Qu, X., Hall, A., Klein, S. A., & Caldwell, P. M. (2014). On the spread of changes in marine low cloud cover in climate model simulations of the 21st century. *Climate Dynamics*, *42*(9–10), 2603–2626. https://doi.org/10.1007/s00382-013-1945-z

Qu, X., Hall, A., Klein, S. A., & Caldwell, P. M. (2015). The strength of the tropical inversion and its response to climate change in 18 cmip5 models. *Climate Dynamics*, *45*(1–2), 375–396. https://doi.org/10.1007/s00382-014-2441-9

Rémillard, J., Kollias, P., Luke, E., & Wood, R. (2012). Marine boundary layer cloud observations in the azores. *Journal of Climate*, *25*(21), 7381–7398. https://doi.org/10.1175/jcli-d-11-00610.1

Rieck, M., Nuijens, L., & Stevens, B. (2012). Marine boundary layer cloud feedbacks in a constant relative humidity atmosphere. *Journal of the Atmospheric Sciences*, *69*(8), 2538–2550. https://doi.org/10.1175/jas-d-11-0203.1

Sherwood, S. C., Bony, S., & Dufresne, J.-L. (2014). Spread in model climate sensitivity traced to atmospheric convective mixing. *Nature*, *505*(7481), 37–42. https://doi.org/10.1038/nature12829

Stephens, G. L., Li, J., Wild, M., Clayson, C. A., Loeb, N., Kato, S., et al. (2012). An update on earth's energy balance in light of the latest global observations. *Nature Geoscience*, *5*(10), 691–696. https://doi.org/10.1038/ngeo1580

Twomey, S. (1974). Pollution and the planetary albedo. *Atmospheric Environment*, *8*(12), 1251–1256. https://doi.org/10.1016/0004-6981(74)90004-3

Vial, J., Dufresne, J.-L., & Bony, S. (2013). On the interpretation of inter-model spread in cmip5 climate sensitivity estimates. *Climate Dynamics*, *41*(11–12), 3339–3362. https://doi.org/10.1007/s00382-013-1725-9

Wang, S., Wang, Q., & Feingold, G. (2003). Turbulence, condensation, and liquid water transport in numerically simulated nonprecipitating stratocumulus clouds. *Journal of the Atmospheric Sciences*, *60*(2), 262–278. https://doi.org/10.1175/1520-0469(2003)060<0262:tcalwt>2.0.co;2

Wentz, F., & Meissner, T. (2004). *Amsr-e/aqua l2b global swath ocean products derived from wentz algorithm, version 2. NASA national snow and ice data center distributed active archive center (Tech. Rep.)*. accessed september 2015. https://doi.org/10.5067/AMSR-E/AE_OCEAN.002

Wood, R. (2012). Stratocumulus clouds. *Monthly Weather Review*, *140*(8), 2373–2423. https://doi.org/10.1175/mwr-d-11-00121.1

Wood, R., & Bretherton, C. S. (2006). On the relationship between stratiform low cloud cover and lower-tropospheric stability. *Journal of Climate*, *19*(24), 6425–6432. https://doi.org/10.1175/jcli3988.1

Zelinka, M. D., Myers, T. A., McCoy, D. T., Po-Chedley, S., Caldwell, P. M., Ceppi, P., et al. (2020). Causes of higher climate sensitivity in cmip6 models. *Geophysical Research Letters*, *47*(1), e2019GL085782. https://doi.org/10.1029/2019gl085782

Zhai, C., Jiang, J. H., & Su, H. (2015). Long-term cloud change imprinted in seasonal cloud variation: More evidence of high climate sensitivity. *Geophysical Research Letters*, *42*(20), 8729–8737. https://doi.org/10.1002/2015gl065911

Zhang, J., Zhou, X., & Feingold, G. (2021). Albedo susceptibility of northeastern pacific stratocumulus: The role of covarying meteorological conditions. *Atmospheric Chemistry and Physics Discussions*, 1–31.

Zhang, M., Bretherton, C. S., Blossey, P. N., Austin, P. H., Bacmeister, J. T., Bony, S., et al. (2013). Cgils: Results from the first phase of an international project to understand the physical mechanisms of low cloud feedbacks in single column models. *Journal of Advances in Modeling Earth Systems*, *5*(4), 826–842. https://doi.org/10.1002/2013ms000246

Zhou, X., Kollias, P., & Lewis, E. R. (2015). Clouds, precipitation, and marine boundary layer structure during the magic field campaign. *Journal of Climate*, *28*(6), 2420–2442. https://doi.org/10.1175/jcli-d-14-00320.1

Reference From the Supporting Information

Sorooshian, A., Feingold, G., Lebsock, M. D., Jiang, H., & Stephens, G. L. (2009). On the precipitation susceptibility of clouds to aerosol perturbations. *Geophysical Research Letters*, *36*(13), L13803. https://doi.org/10.1029/2009GL038993